INVITED PAPER   *Special Section on Distinguished Papers in Photonics*

Wavelength-Switchable Mid-Infrared Narrowband Thermal Emitters Based on Quantum Wells and Photonic Crystals*

Takuya INOUE[†a)], **Menaka DE ZOYSA**[†], **Takashi ASANO**[†], *Nonmembers,* *and* **Susumu NODA**[†], *Member*

SUMMARY   Development of narrowband thermal emitters whose emission wavelengths are dynamically tunable is highly desired for various applications including the sensing of gases and chemical compounds. In this paper, we review our recent demonstration of wavelength-switchable mid-infrared thermal emitters based on multiple quantum wells (MQWs) and photonic crystals (PCs). Through the control of absorptivity by using intersubband transitions in MQWs and optical resonances in PC slabs, we demonstrate novel control of thermal emission, including realization of high-Q ($Q > 100$) thermal emission, dynamic control of thermal emission (~MHz), and electrical wavelength switching of thermal emission from a single device.
key words: *thermal emission, photonic crystals, quantum wells, mid-infrared*

1. Introduction

Thermal emitters generally exhibit a broad spectrum from the terahertz (THz) to the visible region, and have various applications over a wide range of frequencies. However, in many applications such as non-dispersive infrared (NDIR) sensing [1], specific narrowband spectral components are extracted by using optical bandpass filters, leading to an increase of system complexity and a decrease of the power-utilization efficiency of the system. To realize compact and highly efficient systems, it is desired to develop narrowband thermal emitters with minimized background emission, whose emission wavelengths can be tuned according to the targeted wavelength of each application.

The principle of thermal emission control is based on Kirchhoff's law of thermal radiation, which states that the emissivity of an object is equal to the absorptivity [2], [3]. To control the absorptivity of the emitter, optical resonant modes in various types of optical nanostructures including metallic PCs [4], gratings on polar materials [5], and meta-materials [6] have been investigated. Although these structures realized narrowband thermal emission peaks, they also showed undesired background emission outside the targeted wavelengths owing to free carrier absorption in the metals or relatively broadband lattice absorption in polar materials. Besides, there was no way to realize dynamic control of thermal emission with these structures because their absorptive properties were fixed by the materials used. To

overcome these limitations, we recently proposed thermal emission control using intersubband transitions (ISB-Ts) in multiple quantum wells (MQWs) and optical resonances in photonic crystals (PC) slabs [7], [8]. An ISB-T is an electronic transition between two quantized energy levels, which shows a narrowband absorption peak in the mid-infrared range. By properly modifying the well width, barrier height, and doping density of the MQWs, we can arbitrarily change the wavelength and magnitude of absorption. Using these flexible properties, we realized single-peak high-Q ($Q > 100$) thermal emission [9]–[11], dynamic control of thermal emission (~MHz) [12], and electrical wavelength switching of thermal emission [13].

In this paper, we review our recent demonstration of wavelength-switchable mid-infrared narrowband thermal emitters based on MQWs and PCs. In Sect. 2, we briefly review the design strategy to obtain narrowband thermal emission together with the relevant experimental results. In Sect. 3, we report on the experimental demonstration of dynamic thermal emission control, which is the key to the realization of wavelength-switchable mid-infrared thermal emitters. In Sect. 4, we demonstrate the electrical wavelength switching of thermal emission via integration of multiple PCs, and also demonstrate the electrical switching of dual thermal emission peaks using a single PC slab.

2. Realization of High-Q Thermal Emission with MQWs and PCs

2.1 Design Strategy for High-Q Thermal Emitters

Figures 1 (a) and (b) show the basic designs of our narrowband thermal emitters, which consist of GaAs/AlGaAs MQWs and PC slabs. As described in the previous section, we use ISB-Ts in MQWs in order to enhance the absorption coefficient of the material around a target wavelength while suppressing it at other wavelengths. The typical FWHM of the ISB absorption coefficient spectrum is 50–100 cm^{-1}, corresponding to a Q factor of ~10. To obtain a much narrower thermal emission peak in the surface-normal direction, we use the Transverse Magnetic (TM)-like polarized resonant modes at the Γ-point of the photonic band shown in Figs. 1 (c) and (d) (it should be noted that ISB-Ts of MQWs interact only with the electric field perpendicular to the slab). Both an air-hole type PC [Fig. 1 (a)] and a rod-type PC [Fig. 1 (b)] can be utilized for this purpose, but the latter is preferable for achieving single-peak thermal emis-
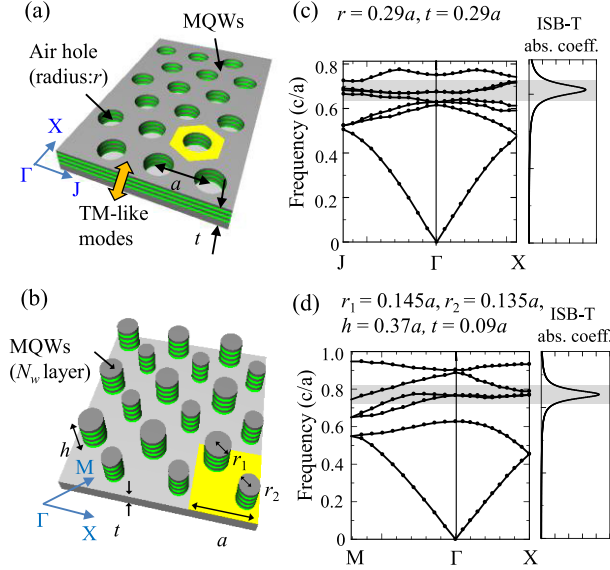
Fig. 1 (a), (b) Basic structure of narrowband thermal emitters based on MQWs and PC slabs (air-hole-type PC and rod-type PC). (c), (d) Photonic band diagrams of the proposed structures for TM-like modes.

sion because of the larger frequency spacing between the Γ-point resonant modes. By matching the resonant wavelength of one of the Γ-point resonances with the ISB-T wavelength as shown in Fig. 1 (d), we can obtain single-peak thermal emission in the surface-normal direction. The angular dependence of the thermal emission spectrum follows the band diagrams shown in Fig. 1 [9], [10], which are less dispersive than that of a surface grating owing to the choice of a relatively flat band. Since we match the ISB-T frequency with the resonant frequency of the Γ-point mode, thermal emission intensity near the surface-normal direction becomes especially high.

The emissivity spectrum obtained from the Γ-point resonant mode is analytically given by

$$\varepsilon^U(\omega) = \frac{\xi}{1+\xi} \times \frac{1/Q_{abs}Q_{rad}}{(\omega/\omega_{res}-1)^2 + (1/2Q_{abs}+1/2Q_{rad})^2},$$
(1)

where ξ is the ratio between the upward and downward emission power, ω_{res} is the angular frequency of the resonant mode, and Q_{abs} and Q_{rad} are the Q factors of the resonant mode determined by the absorption of the ISB-T and by radiation to the surrounding space, respectively [9]. According to Eq. (1), the FWHM of the emissivity spectrum becomes narrower as Q_{abs} and Q_{rad} increase, and the peak emissivity is maximized when the Q matching ($Q_{abs} = Q_{rad}$) is satisfied. Among the above Q factors, Q_{abs} can be controlled by the number of MQW layers (N_w), while Q_{rad} can be adjusted by changing the radii of the air-holes [Fig. 1 (a)] or the rods [Fig. 1 (b)]. It should be noted that air-holes and rods are introduced only in the upper part of the PC slab, so that the resulting vertical asymmetry increases the ratio between the upward and downward emission power (ξ) in Eq. (1).
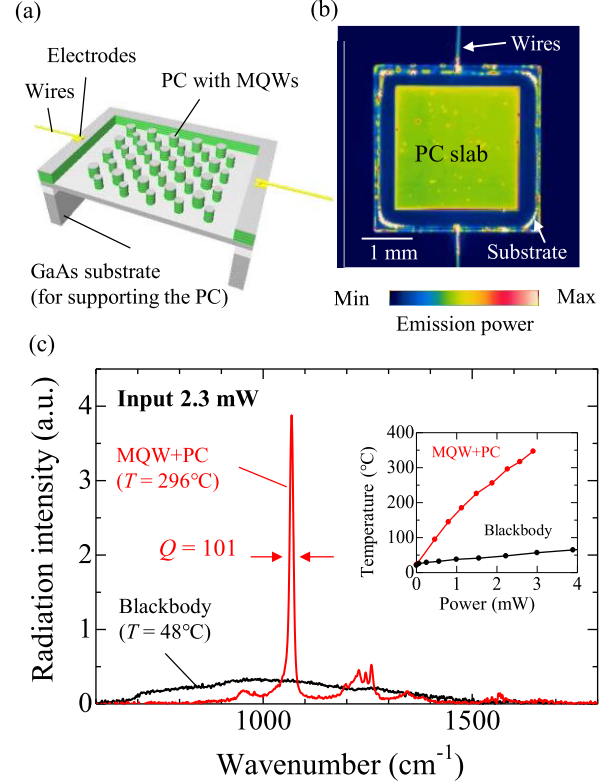

Fig. 2 (a) Schematic of a high-Q thermal emitter based on GaAs/AlGaAs MQWs and a rod-type PC slab. (b) Infrared camera image of the fabricated emitter. (c) Thermal emission spectra of the MQW-PC emitter and the reference blackbody at the same input power. The inset shows the relationship between the emitters' temperature and the input power.

2.2 Experimental Results

In this subsection, we show our recent demonstration of high-Q thermal emitters operating with high power utilization efficiency [11]. The structure of the fabricated PC is based on the rod-type PC shown in Fig. 1 (b), whose structural parameters are set to $N_w = 20$, $h = 2.6\,\mu m$, $t = 0.6\,\mu m$, $a = 7.3\,\mu m$, $r_1 = 0.14a$, and $r_2 = 0.13a$. Each layer of MQWs consists of GaAs (6.8 nm)/Al$_{0.3}$Ga$_{0.7}$As (13.0 nm), where the latter is doped with silicon at a density of $1.0 \times 10^{17}\,cm^{-3}$ to induce an ISB-T at a wavelength of 9.4 μm.

The complete structure of the fabricated emitter is shown in Fig. 2 (a). The device consists of a 2.4 mm × 2.4 mm PC with MQWs, a GaAs substrate frame for supporting the PC slab, and electrodes/electric wires for current injection heating. The size of the whole device including the supporting frame is 3.2 mm × 3.2 mm × 55 μm. To suppress the heat conduction loss through the wires, we suspended the device using two thin nichrome wires (diameter, 15 μm). To suppress the unwanted thermal emission loss from the device, we reduced the volume of the GaAs substrate frame and the area of the electrodes as much as possible. A reference blackbody sample consisting of blackbody paint (JSC-3 Japan Sensor) coated on a GaAs wafer with the same emis-

sion area was also prepared for comparison. The details of the fabrication and characterization of the thermal emitters were reported in our previous paper [11].

Figure 2 (b) shows an infrared camera image of the fabricated device heated by current injection in vacuum ($P < 0.01$ Pa), where enhanced thermal emission is observed from the PC region. Figure 2 (c) shows the measured thermal emission spectra of the MQW-PC emitter and the reference blackbody sample at the same heating power of 2.3 mW. The MQW-PC emitter exhibits a single-mode thermal emission peak with a Q factor of 101 at a wavenumber of 1068 cm^{-1}, while background emission intensity in the other wavelengths is suppressed. The peak intensity of the MQW-PC emitter is 12.6 times higher than that of the reference blackbody at the same input power. This is owing to the suppression of the broadband emission at an unnecessary frequency band, leading to the efficient increase of the device temperature as shown in the inset. The estimated hemispherical thermal emission power at 296°C is 0.27 mW, which is 12% of the input power. This ratio is higher than typical wall-plug efficiencies of commercially available quantum cascade lasers (1~5%), and could be further increased by improving the thermal isolation and enlarging the emission area of the photonic crystal [11].

3. Dynamic Control of Thermal Emission

3.1 Principle and Device Structure for Dynamic Thermal Emission Control

The response speed of conventional thermal emitters is very slow because their emission intensity is determined only by the temperature, which is difficult to modulate fast. However, according to Kirchhoff's radiation law, radiation intensity of thermal emitters is determined not only by the temperature but also by the absorptivity of the emitters. Therefore, by rapidly changing the absorptivity, we can achieve much faster control of thermal emission than that using the conventional temperature-modulation method.

Figure 3 (a) shows a schematic picture of a thermal emitter that enables dynamic control of thermal emission [12], [14]. The device consists of n-doped GaAs/Al$_{0.3}$Ga$_{0.7}$As MQWs grown between an n-type GaAs layer and a p-type GaAs layer, where an air-hole type PC is introduced. As we described in the previous section,
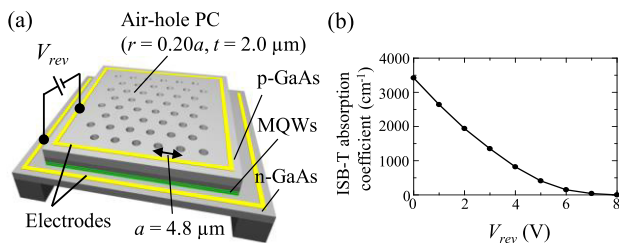
the MQWs induce narrowband absorption around the transition wavelength of the ISB-T. The magnitude of the absorption coefficient can be externally controlled by changing the electron density in the quantum wells by applying a reverse bias to the p-n diode. Figure 3 (b) shows the calculated intersubband absorption coefficient of the MQWs as a function of reverse bias [12], [14], where a reverse bias of 8 V is enough for reducing the intersubband absorption coefficient to zero. This large change in the absorption coefficient is the key for the dynamic control of absorptivity (emissivity). The lattice constant (4.8 μm) and air-hole radius (0.96 μm) of the PC slab were adjusted so that a thermal emission peak with a high Q factor and a high emissivity is obtained from one of the Γ-point resonant modes, as described in Sect. 2.1.

3.2 Experimental Results

Figure 4 (a) shows the thermal images of the fabricated device with a 1.8 mm × 1.8 mm PC with and without an applied reverse bias of 10 V. The device temperature was fixed at 100°C, and the spatial distribution of thermal emission was observed using a thermal imaging camera. The thermal radiation power emitted from the PC slab uniformly decreased when a reverse bias of 10 V was applied. Next, we measured the thermal emission spectra of the same device heated at 200°C in the surface normal direction using the FTIR spectrometer. Figure 4 (b) shows the measured
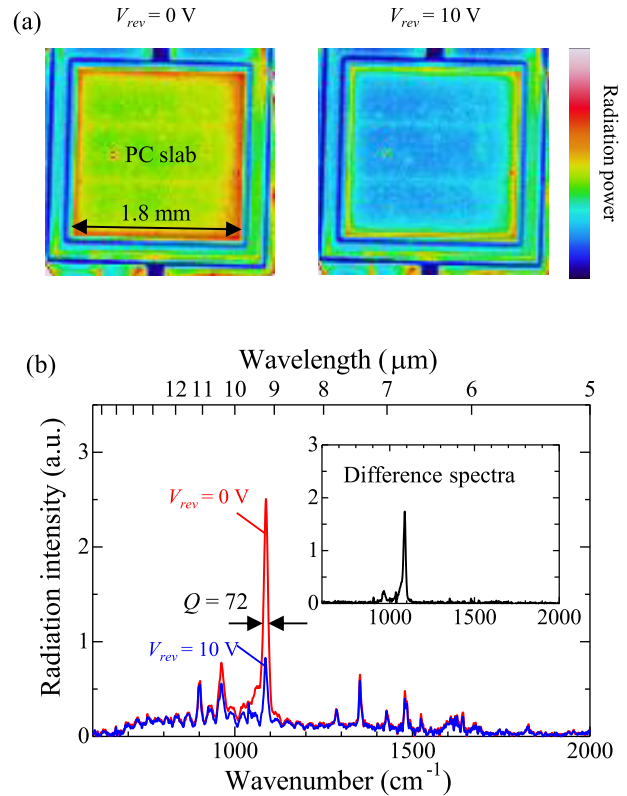
Fig. 3 (a) Schematic of the thermal emitter for dynamic thermal emission control. (b) Calculated ISB absorption coefficient of the MQWs as a function of reverse bias.

Fig. 4 (a) Thermal images of the fabricated device at 100°C with and without reverse bias. (b) Thermal emission spectra at 200°C with and without reverse bias. The difference spectrum is shown in the inset.
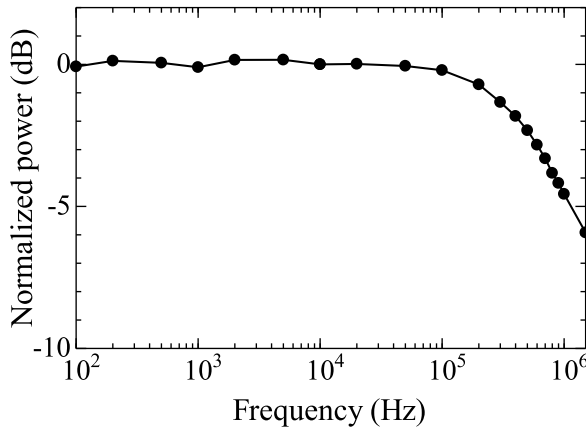
Fig. 5 Frequency characteristic of the modulated thermal emission power of the fabricated device.
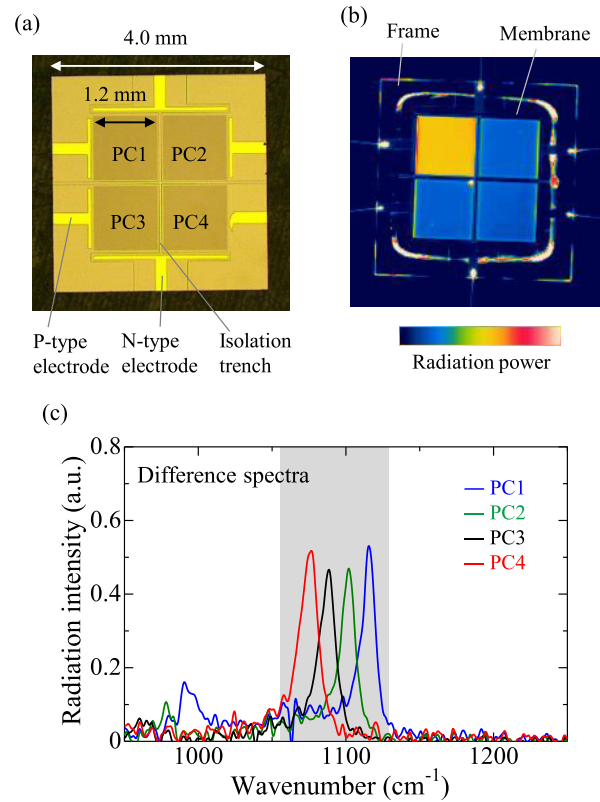

Fig. 6 (a) Microscope image of the device with four MQW-PC emitters for electrical switching of thermal emission wavelengths. (b) Thermal image of the fabricated device at a heating power of 3.6 mW. (c) Difference spectra with and without a reverse bias for the fabricated device. The FWHM of the ISB-T spectrum is superimposed in gray.

spectra with and without a reverse bias of 10 V. Without reverse bias, the device exhibited a narrowband thermal emission peak ($Q = 72$) at a wavenumber of $1088\,\mathrm{cm}^{-1}$. With a reverse bias of 10 V, the intensity of the main emission peak decreased to one third. The emission remained at a reverse bias of 10 V was caused by the free-carrier absorption (emission) in the contact layers (p-GaAs/n-GaAs). Several smaller side-peaks appeared in addition to the main peak, which were caused by the other Γ-point resonant modes of the air-hole type PC. However, the intensity change of these side-peaks caused by the reverse bias was smaller than that of the main peak as shown in the difference spectra [inset of Fig. 4 (b)] owing to the larger frequency detuning from the ISB-T wavenumber.

We also investigated the dynamic performance of the fabricated device by applying a square voltage alternating between 0 V to 10 V with various modulation frequency. The temporal variation in the thermal emission power was measured using a HgCdTe detector and a lock-in-amplifier. The measured frequency characteristics of the device are shown in Fig. 5. The 3 dB cutoff frequency reaches 600 kHz, which is four orders of magnitude faster than that of conventional fast thermal emitters adopting a temperature-modulation method. The response speed of our device is limited by the RC time constant of the electrical circuit, which is determined by the in-plane resistance of the p-GaAs/n-GaAs layers, the depletion layer capacitance, and the device size. Calculations taking account of these factors revealed that the 3 dB cutoff frequency of the fabricated device (2 mm × 2 mm) was around 1 MHz, which agrees well with the above experimental result. Moreover, by reducing the device size to 0.5 mm × 0.5 mm, the expected bandwidth exceeds 10 MHz due to the shorter distance travelled by the carriers.

4. Development of Wavelength-Switchable Narrowband Thermal Emitters

In this section, we demonstrate two methods for electri-

cal wavelength switching of narrowband thermal emitters, which will be beneficial for various mid-infrared sensing applications.

4.1 Electrical Wavelength Switching of Thermal Emission via Integration of Multiple PCs

The first method to realize wavelength-switching of thermal emission is straightforward; we integrate multiple thermal emission devices emitting at different wavelengths on a single chip, and dynamically change the thermal emission intensity of each device one by one. Although the idea is very simple, such wavelength-switching operation was impossible to achieve with conventional thermal emitters due to the lack of methods for high-speed control of thermal emission intensity.

Figure 6 (a) shows a microscope image of a fabricated device for the electrical switching of thermal emission wavelengths [13]. Here, four MQW-PC emitters with different lattice constants (a = 4.6, 4.7, 4.8, and 4.9 μm) are integrated on a single chip. The area of each emitter is 1.2 × 1.2 mm². The structure of each MQW-PC emitter is the same as that shown in Fig. 3 (a), the emission intensity of which can be dynamically controlled by applying reverse bias between p-GaAs and n-GaAs. The four emit-
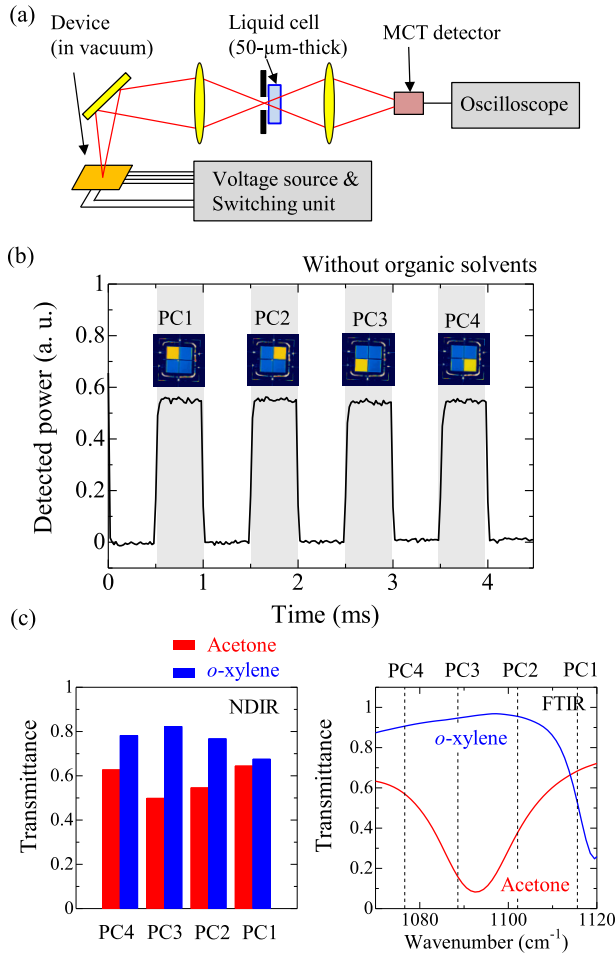
Fig. 7 (a) Experimental setup for NDIR sensing using a wavelength-switchable narrowband thermal emitter. (b) Temporal thermal emission power waveform measured by MCT detector. (c) Transmittance of acetone (red) and o-xylene (blue) measured using NDIR setup (left) and FTIR (right).

Fig. 8 (a) Schematic of a two-wavelength switchable PC thermal emitter. (b) Measured transmission spectrum of the flat MQW wafer. The FWHMs of the ISB-T absorption spectra are shown in blue and pink.

MQW-PC emitter is shown. Narrowband ($Q > 70$) thermal emission peaks were obtained at four different wavelengths within the FWHM of the ISB-T absorption coefficient spectrum (shown in gray).

Using the above wavelength-switchable narrowband thermal emitter, we performed a simple demonstration of non-dispersive infrared (NDIR) sensing of organic solvents. Figure 7 (a) shows the experimental setup for NDIR sensing. The thermal emission from each MQW-PC emitter was turned on one by one for 0.5 ms, passed through a liquid cell filled with organic solvents (acetone or o-xylene, path length: 50 μm), and was detected using an MCT detector and a digital oscilloscope. It should be noted that the above system is much simpler than that of a conventional NDIR system, which usually involves broadband light sources such as a blackbody-like thermal emitter, a mechanical chopper for synchronous detection of light, multiple narrowband optical filters whose pass-bands cover the absorption lines of the target materials, and multiple detectors. Figure 7 (b) shows the temporal response of the detected thermal emission power without organic solvents. Here, four successive emission pulses corresponding to the four different wavelengths shown in Fig. 6 (c) were obtained within a short time (4 ms). Next, we filled the liquid cell with acetone or o-xylene and measured the decrease in detected power for the above four wavelengths. The measured transmittance of the four emission pulses is shown in the left panel of Fig. 7 (c). For comparison, the transmission spectra measured by FTIR is shown in the right panel. The wavelength-

ters are electrically insulated by an insulation trench running through the p-GaAs layer, which enables individual control of the thermal emission intensity of each PC. A p-type electrode for applying the control bias was deposited on the side of each emitter, and two n-type electrodes were deposited at the top and bottom of the device for heating the device by current injection. Six thin electric wires were attached to the device to suspend it so that heat conduction losses during current injection are minimized. Figure 6 (b) shows an infrared camera image of the fabricated device at a heating power of 3.6 mW in a vacuum chamber (< 0.01 Pa). A reverse bias of -8 V is applied to three of the four PCs. Here, thermal emission from one PC is selectively "switched on" and emission from the other three is "switched off". The switching speed of the device is above 10 kHz, which is much faster than the speed of the temperature response. Figure 6 (c) shows the thermal emission spectra of the fabricated device in the surface-normal direction, where the difference between the spectrum measured with no reverse bias and that obtained on applying a reverse bias of 8 V to each
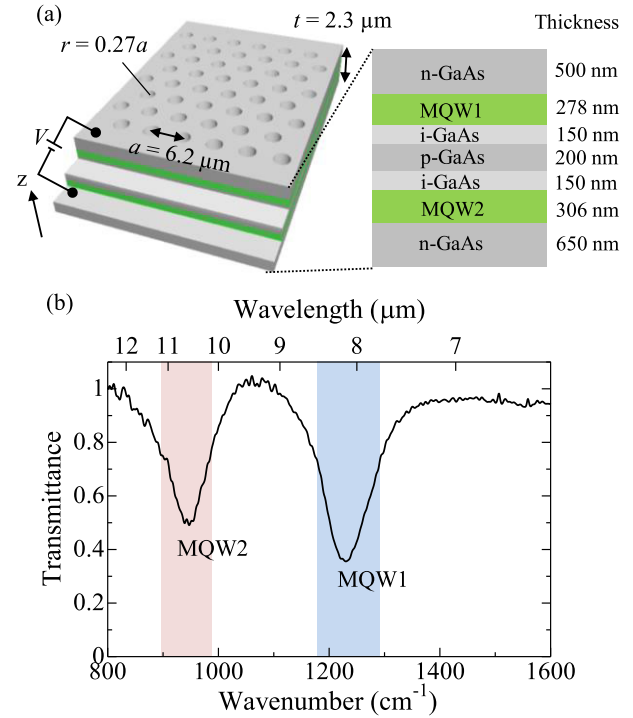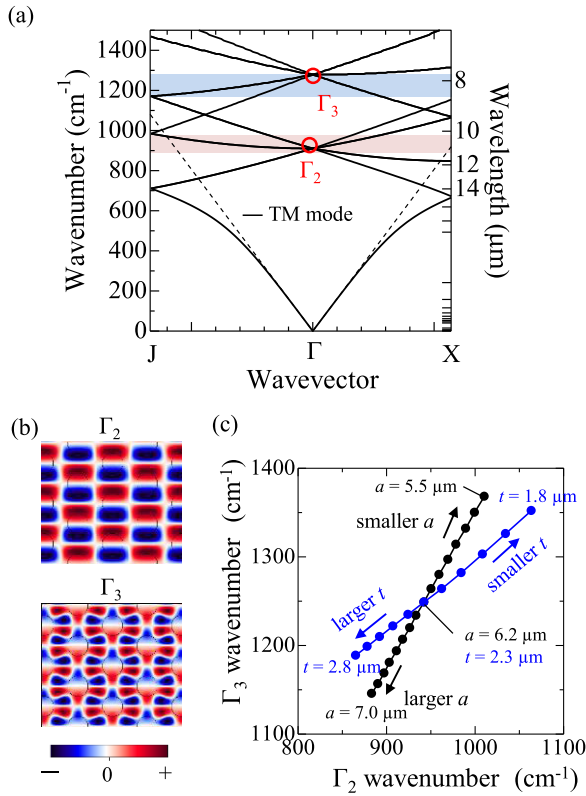
Fig. 9 (a) Photonic band of the designed PC for TM-polarized modes, calculated by empty-lattice approximation. The FWHMs of the absorption spectra (Fig. 8) are shown in blue and pink. (b) Electric field distribution (E_z) of the Γ_2 and Γ_3 modes. (c) Wavenumber shift of the Γ_2 and Γ_3 modes due to the change of the lattice constant and thickness of the PC slab.
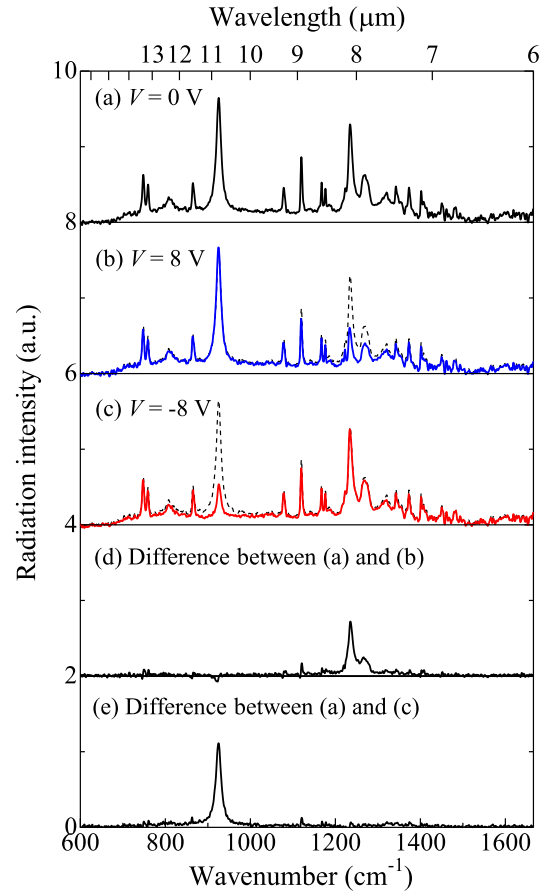

Fig. 10 Measured thermal emission spectra of the fabricated device at 150°C in the surface-normal direction: (a) without bias, (b) with a positive bias of 8 V, (c) with a negative bias of 8 V. (d) Difference between the spectrum without a bias and that with a positive bias of 8 V. (e) Difference between the spectrum without a bias and that with a negative bias of 8 V.

dependent transmittance of acetone/o-xylene was clearly observed even in the case of the NDIR experiment. The quantitative difference between the transmittance measured by NDIR and by FTIR is caused by the finite broadening of the emission spectra, which can be reduced by optimizing the design of the MQW-PC emitters.

4.2 Electrical Switching of Dual Thermal Emission Peaks Using a Single PC Slab

In the device demonstrated in the previous subsection, the number of thermal emission wavelengths that can be switched is limited by the number of the MQW-PC emitters that can be integrated. Besides, the range of the wavelength switching is relatively narrow ($\sim$50 cm^{-1}), which is limited by the width of the ISB-T absorption coefficient spectrum of the MQWs. In order to realize the switching of more emission peaks across a broader wavelength range, we next investigate an emitter that enables switching of dual thermal emission peaks at two distant wavelengths from a single light-emitting surface.

Figure 8 (a) shows the schematic of the proposed emitter, which consists of two GaAs/Al$_{0.34}$Ga$_{0.66}$As MQWs incorporated inside n-GaAs/p-GaAs/n-GaAs layers and a single air-hole PC slab. The two MQWs have different well

widths (5.9 nm and 7.9 nm) so that ISB-T absorption at two distant wavelengths in the mid-infrared range are induced. Figure 8 (b) shows the measured transmission spectrum of the MQW wafer without a PC structure for edge-incident TM-polarized light, where narrowband absorption peaks are observed at two distant wavelengths (8.1 μm and 10.5 μm). When a positive (negative) bias V is applied between the top n-GaAs and the bottom n-GaAs layer as shown in Fig. 8 (a), the electrons inside the MQW1 (MQW2) are extracted due to the expansion of the depletion layer of the upper (lower) pn junction. This leads to the selective quenching of the ISB-T at each wavelength.

Figure 9 (a) shows the photonic band structure of the designed air-hole PC for TM-polarized modes, calculated by approximating the PC slab as a uniform slab with the same average refractive index (empty-lattice approximation). To obtain dual emission peaks from a single PC slab, we utilize not only the Γ-point resonant mode with the lowest frequency (Γ_2 resonance) but also the higher-order Γ-point resonant mode (Γ_3 resonance). The electric field distributions (E_z) of these resonant modes are shown in Fig. 9 (b). The lattice constant (a) and thickness (t) of the PC slab are ad-

justed so that these modes interact with the ISB-T of the two MQWs to yield dual high-Q thermal emission peaks in the surface-normal direction. As shown in Fig. 9 (c), we can change the resonant wavelengths (wavenumbers) of the Γ_2 and Γ_3 modes in a wide range by changing the lattice constant or thickness (or both).

The measured thermal emission spectra of the fabricated device with a 2.4 mm × 2.4 mm PC slab at 150°C in the surface-normal direction are shown in Figs. 10 (a)–(c). The device with no bias shows two main emission peaks around the two ISB-T wavelengths (8.1 μm and 10.8 μm). When the positive (negative) bias is applied between the top n-GaAs and the bottom n-GaAs layer, the intensity of the emission peak at the shorter (longer) wavelength selectively decreases. Several small peaks also appear away from the ISB-T wavelengths, which may be caused by the free carriers in the p-GaAs/n-GaAs layers, but the intensity of these peaks does not change with an applied bias. The difference of the spectra with and without a bias is shown in Figs. 10 (d) and 10 (e). By modulating the applied bias, almost monochromatic thermal emission was obtained at each of the two wavelengths from a single light-emitting surface. It should be noted that our device is much simpler than other mid-infrared wavelength-switchable light sources such as external-cavity quantum cascade lasers.

5. Conclusions

In this paper, we have reported on the demonstration of wavelength-switchable mid-infrared narrowband thermal emitters based on MQWs and PCs. By controlling the absorptivity of the emitter using ISB-Ts in MQWs and Γ-point resonant modes in PC slabs, we have realized monochromatic high-Q thermal emitters that operate with very low power consumption, and dynamic control of thermal emission that is four orders of magnitude faster than is possible using conventional temperature modulation. Furthermore, we have demonstrated electrical switching of thermal emission wavelengths in the mid-infrared range by integrating multiple MQW-PC emitters and also by using a single PC emitter interacting with two different MQWs. Our devices will greatly contribute to the miniaturization of infrared sensing systems because they enable direct modulation of thermal emission power and on-chip switching of emission wavelengths without using any mechanical choppers or optical bandpass filters. We hope that our demonstrations will accelerate the application of mid-infrared thermal emitters in various fields such as environmental monitoring, bio-sensing, and medical diagnosis.

Acknowledgments

References

[1] J. Meléndez, A.J. de Castro, F. López, and J. Meneses, "Spectrally selective gas cell for electrooptical infrared compact multigas sensor," Sensors and Actuators A, vol.47, no.1, pp.417–421, 1995.

[2] J.-J. Greffet and M. Nieto-Vesperinas, "Field theory for generalized bidirectional reflectivity: derivation of Helmholtz's reciprocity principle and Kirchhoff's law," J. Opt. Soc. Am., vol.15, no.10, pp.2735–2744, 1998.

[3] T. Inoue, M.D. Zoysa, T. Asano, and S. Noda, "Realization of narrowband thermal emission with optical nanostructures," Optica, vol.2, no.1, pp.27–35, 2015.

[4] V. Rinnerbauer, Y.X. Yeng, W.R. Chan, J.J. Senkevich, J.D. Joannopoulos, M. Soljačić, and I. Celanovic, "High-temperature stability and selective thermal emission of polycrystalline tantalum photonic crystals," Opt. Express, vol.21, no.9, pp.11482–11491, 2013.

[5] J.-J. Greffet, R. Carminati, K. Joulain, J.-P. Mulet, S. Mainguy, and Y. Chen, "Coherent emission of light by thermal sources," Nature, vol.416, no.6876, pp.61–64, 2002.

[6] X. Liu, T. Tyler, T. Starr, A.F. Starr, N.M. Jokerst, and W.J. Padilla, "Taming the blackbody with infrared metamaterials as selective thermal emitters," Phys. Rev. Lett., vol.107, no.4, 045901, 2011.

[7] T. Asano, K. Mochizuki, M. Yamaguchi, M. Chaminda, and S. Noda, "Spectrally selective thermal radiation based on intersubband transitions and photonic crystals," Opt. Express, vol.17, no.21, pp.19190–19202, 2009.

[8] M.D. Zoysa, T. Asano, K. Mochizuki, A. Oskooi, T. Inoue, and S. Noda, "Conversion of broadband to narrowband thermal emission through energy recycling," Nature Photon., vol.6, no.8, pp.535–539, 2012.

[9] T. Inoue, T. Asano, M.D. Zoysa, A. Oskooi, and S. Noda, "Design of single-mode narrow-bandwidth thermal emitters for enhanced infrared light sources," J. Opt. Soc. Am. B, vol.30, no.1, pp.165–172, 2013.

[10] T. Inoue, M.D. Zoysa, T. Asano, and S. Noda, "Single-peak narrow-bandwidth mid-infrared thermal emitters based on quantum wells and photonic crystals," Appl. Phys. Lett., vol.102, no.19, 191110, 2013.

[11] T. Inoue, M.D. Zoysa, T. Asano, and S. Noda, "High-Q mid-infrared thermal emitters operating with high power-utilization efficiency," Opt. Express, vol.24, no.13, pp.15101–15109, 2016.

[12] T. Inoue, M.D. Zoysa, T. Asano, and S. Noda, "Realization of dynamic thermal emission control," Nature Mater., vol.13, no.10, pp.928–931, 2014.

[13] T. Inoue, M.D. Zoysa, T. Asano, and S. Noda, "On-chip integration and high-speed switching of multi-wavelength narrowband thermal emitters," Appl. Phys. Lett., vol.108, no.9, 091101, 2016.

[14] T. Inoue, M.D. Zoysa, T. Asano, and S. Noda, "Electrical tuning of emissivity and linewidth of thermal emission spectra," Phys. Rev. B, vol.91, no.23, 235316, 2015.

Takuya Inoue received B.S., M.S., and Ph.D. degrees from Kyoto University, Kyoto, Japan, in 2012, 2014, and 2016, respectively, all in electronic science and engineering. From 2014 to 2016, he was a Research Fellow of the Japan Society for the Promotion of Science at Kyoto University. Since 2016, he is an Assistant Professor in the Department of Electronic Science and Engineering, Kyoto University. His current research interest covers the fundamental control of thermal emission and the development of novel light sources using photonic crystals.

Menaka De Zoysa received B.S., M.S. and Ph.D. degrees in Electronic Science and Engineering from Kyoto University, Kyoto, Japan, in 2007, 2009 and 2012 respectively. From 2010 to 2012, he was a Research Fellow of the Japan Society for the Promotion of Science with Kyoto University. From 2012 to 2014, he was a Postdoctoral fellow in the Quantum Optoelectronics Laboratory. From 2014 to 2016, he was an Assistant Professor at the Hakubi Center for Advanced Research, Kyoto University. He is currently a Senior Lecturer at Department of Electronic Science and Engineering. His research interests include thermal emission control based on manipulation of electronic and photonic states, development of photonic crystal introduced thin-film solar cells, and development and improvement of photonic crystal lasers.

Takashi Asano received B.S., M.S., and Ph.D. degrees from Kyoto University, Kyoto, Japan, in 1992, 1994, and 1997, respectively, all in electronics. From 1996 to 1998, he was a Research Fellow with the Japan Society for the Promotion of Science at Kyoto University. From 1999 to 2000, he was a Postdoctoral Fellow at the Kyoto University Venture Business Laboratory, Kyoto. He joined Kyoto University, in 2000, and is currently an Associate Professor in the Department of Electronic Science and Engineering. His research has been concerned with intersubband transitions in quantum wells, ultrafast phenomena in semiconductors, and 2-D photonic crystals. His current research interest includes photon manipulation using high-Q photonic nanocavities, SiC photonics, and thermal radiation control using semiconductor quantum structures and 2-D photonic crystals. He received an Encouragement Prize of the Japan Society of Applied Physics (1999).

Susumu Noda received B.S., M.S., and Ph.D. degrees from Kyoto University, Kyoto, Japan, in 1982, 1984, and 1991, respectively, all in electronics. In 2006, he has received an honorary degree from Gent University, Gent, Belgium. From 1984 to 1988, he was with the Mitsubishi Electric Corporation, and he joined Kyoto University in 1988. Currently he is a full Professor with the Department of Electronic Science and Engineering and a director of Photonics and Electronics Science and Engineering Center (PESEC), Kyoto University. His research interest covers physics and applications of photonic nanostructures based on photonic crystals. Prof. Dr. Noda is the recipient of various awards, including the IBM Science Award (2000), the Japan Society of Applied Physics Achievement Award on Quantum Electronics (2005), Optical Society of America Joseph Fraunhofer Award/Robert M. Burley Prize (2006), 1st Japan Society of Applied Physics Fellow (2007), IEEE Fellow (2008), The Commendation for Science and Technology by the Minister of Education, Culture, Sports, Science and Technology (2009), IEEE Nanotechnology Pioneer Award (2009), The Leo Esaki Award (2009), Medal with Purple Ribbon (2014), and the Japan Society of Applied Physics Outstanding Achievement Award (2015).